Nanoscale

Accepted Manuscript

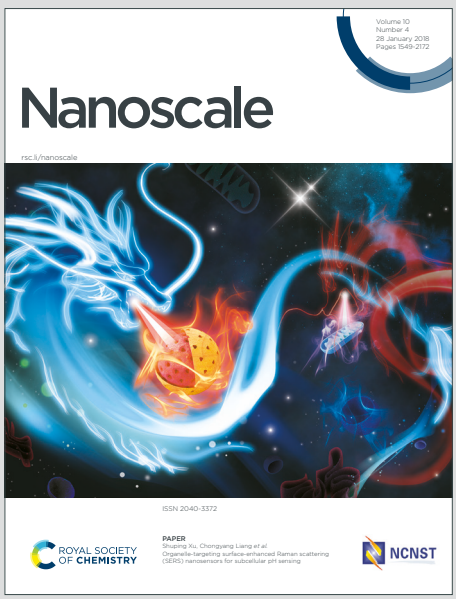

ROYAL SOCIETY OF CHEMISTRY

rsc.li/nanoscale

COMMUNICATION

The influence of dysfunctional actin on polystyrene-nanotube-mediated mRNA nanoinjection into mammalian cells

Received 00th January 20xx,
Accepted 00th January 20xx

DOI: 10.1039/x0xx00000x

Hao Zhe Yoh[1,2,3†], Yaping Chen[1†*], Ali-Reza Shokouhi[1,2], Helmut Thissen[3], Nicolas H. Voelcker[1,2,4*], Roey Elnathan[1,2,5,6,7*]

The advancement of nanofabrication technologies has transformed the landscape of engineered nano–bio interfaces, especially with vertically aligned nanoneedles (NNs). This enables scientists to venture into new territories, widening NN applications into increasingly more complex cellular manipulation and interrogation. Specifically, for intracellular delivery application, NNs have shown to mediate the delivery of various bioactive cargos into a wide range of cells—a physical method termed "nanoinjection". Silicon (Si) nanostructures demonstrated great potential in nanoinjection, whereas the use of polymeric NNs for nanoinjection has rarely been explored. Furthermore, the underlying mechanism of interaction at the cell–NN interface is subtle and multifaceted, and not fully understood—underpinned by the design versatility of the NN biointerface. Recent studies have suggested that actin dynamic plays a pivotal role influencing the delivery efficacy. In this study, we fabricated a new class of NNs—a programmable polymeric nanotubes (NTs) — from polystyrene (PS) cell cultureware, designed to facilitate mRNA delivery into mouse embryonic fibroblast GPE86 cells. The PSNT delivery platform was able to mediate mRNA delivery with high delivery efficiency (~83%). We also investigated the role of actin cytoskeleton in PSNTs mediated intracellular delivery by introducing two actin inhibitors—cytochalasin D (Cyto D) and jasplakinolide (Jas)—to cause dysfunctional cytoskeleton, via inhibiting actin polymerization and depolymerization, respectively (before and after the establishment of cell–PSNT interface). By inhibiting actin dynamics 12 h before cell–PSNT interfacing (pre-interface treatment), the mRNA delivery efficiencies were significantly reduced to ~3% for Cyto D-treated samples and ~1% for Jas-treated sample, as compared to their post-interface (2 h after cell–PSNT interfacing) counterpart (~46% and ~68%, respectively). The added flexibility of PSNTs have shown to help withstand mechanical breakage stemming from cytoskeletal forces in contrast to the SiNTs. Such findings will step-change our capacity to use programmable polymeric NTs in fundamental cellular processes related to intracellular delivery.

Introduction

The advancement of nanofabrication alongside with nanobiotechnology in the recent years has enhanced the engineered nano–bio cellular interfaces and widened their applications.[1-6] In particular, vertically aligned nanoneedles (NNs) of semiconducting, inorganic, and polymeric materials—such as nanowires,[7-10] nanostraws,[11, 12] nanotubes (NTs),[13-16] and their electroactive analogues,[17-19]—have shown to be promising tools for complex cellular manipulation, such as mechanotransduction,[20-25] biosensing,[26, 27] immunomodulation,[28] *in vivo* and *ex vivo* gene editing,[29-32] intracellular delivery,[33-39] and even cellular reprogramming.[40-42]

Fabrication complexity [43-48] and physico-chemical properties [49, 50] of the of NNs depends on the selection of materials and various fabrication pathways. For example, silicon (Si) NNs can offer high precision in their fabrication but require more complex fabrication protocols, resulting limited throughput of fabrication.[51] By contrast, NNs made of polymeric materials—such as polystyrene (PS) and SU8—provide highly reproducible, cost-effective, and rapid fabrication pathways that allow high-throughput manufacturing capacity.[23, 38, 52, 53] Most polymeric NNs have high optical transparency, biocompatibility, and flexibility in chemical modifications—all of which are beneficial

†Hao Zhe Yoh and Yaping Chen contributed equally.
[1]Monash Institute of Pharmaceutical Sciences, Monash University, 381 Royal Parade, Parkville, VIC 3052, Australia
[2]Melbourne Centre for Nanofabrication, Victorian Node of the Australian National Fabrication Facility, 151 Wellington Road, Clayton, VIC 3168, Australia
[3]Commonwealth Scientific and Industrial Research Organization (CSIRO), Clayton, VIC 3168, Australia
[4]Department of Materials Science and Engineering, Monash University, 22 Alliance Lane, Clayton, VIC 3168, Australia.
[5]School of Medicine, Faculty of Health, Deakin University, Waurn Ponds, Geelong, VIC 3216, Australia.
[6]Institute for Frontier Materials, Deakin University, Geelong Waurn Ponds campus, Geelong, VIC 3216, Australia.
[7]Institute for Innovation in Mental and Physical Health and Clinical Translation (IMPACT), Geelong Waurn Ponds campus, Geelong, VIC 3216, Australia.

for a large variety of cellular manipulation and interrogations applications.[54-56]

One key application of NNs is intracellular delivery, also known as nanoinjection, which allows the delivery of diverse bioactive cargoes into mammalian cells and tissues.[5, 57] Semiconducting or metal NNs have mainly been utilized for nanoinjection, whereas polymeric NNs have been rarely exploited for such application.[38] Although NNs were shown as effective nanoinjection tools, the mechanism of nanoinjection is still subject to debate.[1, 58, 59] Mechanisms such as spontaneous penetration,[60, 61] membrane permeabilization,[18, 62] and NN-mediated endocytosis [7, 37] were proposed. Due to the intricacy of cell–NN interaction involving complex biochemical and biophysical cues, a better understanding of such interaction is crucial for establishing smart nano–bio interface for maximizing biocargo delivery with minimal perturbation.[57]

The actin cytoskeleton is an important component that participate in many cellular functions, such as controlling cell morphology and motility, promoting axonal growth, and regulating membrane trafficking.[63] Upon interfacing with NNs, cytoskeletal components can regulate cytosolic entry and cargo delivery by generating membrane deformations and mechanotransduction.[64, 65] When cell adhered onto NNs, the force generated by cell adhesion can influence the tension on plasma membrane and alter cell permeability.[66] Interestingly, the effect of actin dynamics on cell permeability varies throughout the cell–NN interfacing period. For example, at the beginning of cell–NN interfacing, direct access to the cellular interior compartment is favorable, resulting from a local NN-induced deformation and actin reorganization.[23, 67] However, once a stable actin meshwork at the cell–NN interface is established, endocytic processes are more favorable due to the recruitment of curvature-sensitive proteins at the interface.[68]

In this study we fabricated for the first time vertically-aligned PSNT arrays and investigated the role of actin cytoskeleton in PSNT-mediated mRNA delivery into mouse fibroblast (GPE86) cells. Actin dynamics were disrupted by introducing two actin inhibitors—cytochalasin D (Cyto D) and jasplakinolide (Jas)—to induce dysfunction of the actin cytoskeleton within GPE86 cells. We demonstrated that this new class of PSNTs can mediate intracellular delivery, achieving mRNA delivery efficiency of ~83% for untreated cells. Interestingly, the delivery efficiency is significantly reduced for the pre-interface samples treated by either Cyto D or Jas (~3% and ~1%, respectively), as compared to their post-interface counterpart (~46% and ~68%, respectively). This finding demonstrates the capability of PSNTs for mediating biomacromolecule delivery, negating NT breakage due to cellular forces, and simultaneously revealing the significance of actin cytoskeleton in facilitating intracellular delivery for the nascent cell–PSNT interface.

Results and Discussions

Engineered SiNT arrays of precise geometry were used as master template for polymeric NT replication. The SiNT arrays were fabricated by using e-beam lithography (EBL) and reactive ion etching (DRIE) as described in our previous work.[14] A thin film of octafluorocyclobutane (C_4F_8)—Teflon-like polymer—was deposited on the SiNT master as an anti-adhesive layer via plasma polymerization (**Figure 1a i**). This anti-adhesive layer ensures efficient master template removal after the casting process. Hard polydimethylsiloxane (h-PDMS) was spin-coated on the master template, followed by a layer of PDMS to create a h-PMDS/PDMS composite that functions as a negative mold for PSNT replication (Figure 1a ii-iii). A thin film of the same anti-adhesive layer was deposited by plasma polymerization on the negative mold prior to PSNT replication.

Thermal nanoimprint lithography (thermal-NIL) was used to replicate the PSNTs. A flat PS cell cultureware substrate was placed on top of a Si wafer backing to maintain the flatness of the PS substrate and to ensure efficient heat transfer (figure 1b i). Next, the pre-fabricated negative mold was placed in contact with the PS substrate under constant imprinting pressure. The substrate was heated above its glass transition temperature during the molding stage (Figure 1b ii). Constant pressure was maintained until PSNTs were cooled to set and the mold was removed to obtain the replicated PSNTs (Figure 1b iii). The replicated PSNTs imaged by means of scanning electron microscopy (SEM) showed good NT coverage (Figure 1c i) with successful replication of hollow structures (Figure 1c ii) from the SiNT master. The PSNT arrays consist of inner/outer diameter of 500/900 nm, height of 2 µm, and pitch of 5 µm (Figure 1c iii). The hollow structure of the PSNTs was further examined by performing focused ion beam (FIB) milling to reveal the cavities inside the NTs (Figure 1c iv). This opening is crucial for loading controlled amount of bio-cargos without any surface functionalization. The PSNT arrays were cleaned and treated with air plasma to enhance its hydrophilicity, then UV sterilized before loading with Cy5-tagged and GFP encoded mRNA. To verify the loading of mRNA in PSNTs, confocal laser microscopy imaging was used. Cy5 signal was observed inside the cavities of PSNTs (Figure S1a) across the sample (Figure S1b), indicating successful loading of mRNA.

The actin cytoskeleton is a crucial component for maintaining cell morphology, adhesion, signaling and migration, which in turn can influence intracellular delivery efficacy.[63] Adherent mouse embryonic fibroblast (GPE86) cells were treated with two types of actin inhibitors—Cyto D or Jas—to study the role of actin in PSNT-mediated intracellular delivery. Cyto D is a fungal metabolite that has high affinity binding to the growing ends of F-actin, resulting severe disruption of actin network organization and inhibition of actin polymerization.[69] Jas is a naturally occurring cyclo-depsipeptide from a marine sponge, which acts as an actin stabilizer by binding to the side of actin filaments, inducing actin polymerization while inhibiting depolymerization.[70]

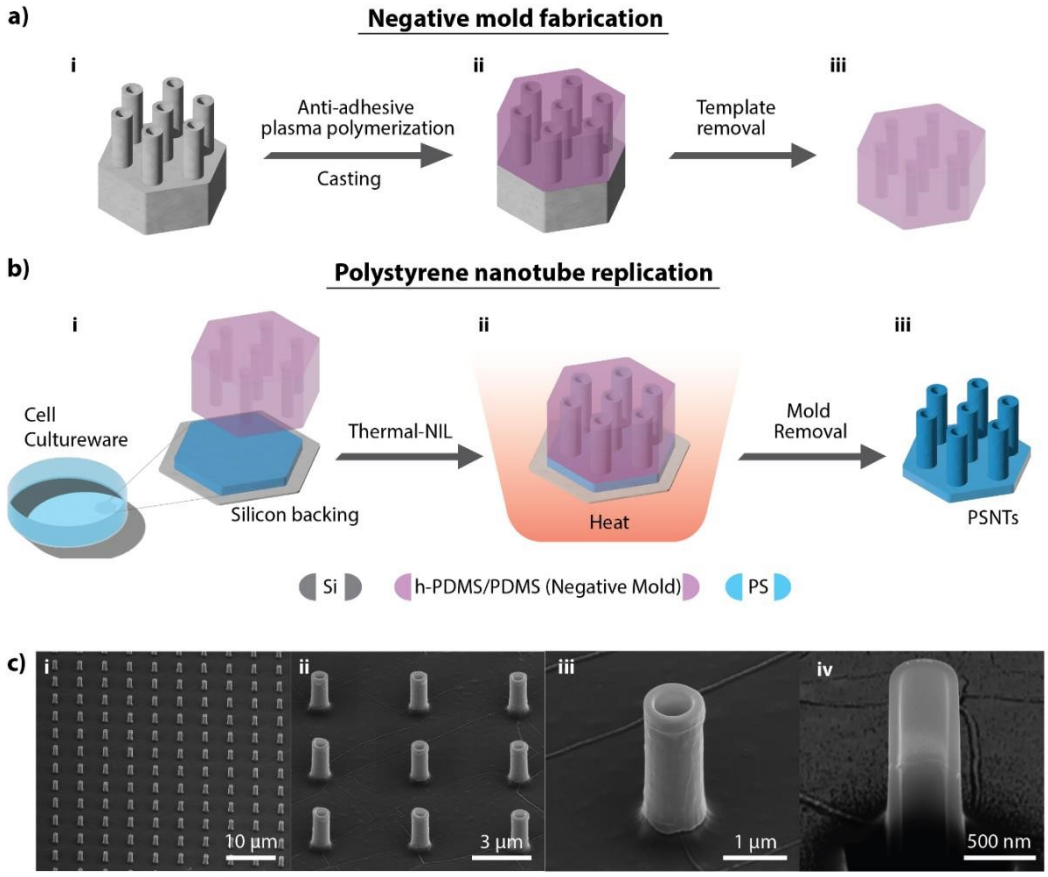

Figure 1. PSNT fabrication workflows. *(a) Negative mold fabrication.* (i) The SiNTs master template was first deposited an anti-adhesive layer by plasma polymerization deposition and (ii) casted with h-PDMS/PDMS composite, which was left to cure. (iii) The SiNT master template was removed after curing to obtain the negative mold. A thin film of the same anti-adhesive was deposited to the negative mold prior to PSNT replication. *(b) PSNT replication.* (i) The PS substrate from cell cultureware was prepared and placed on top of a Si backing, then (ii) pressed by the negative mold during thermal-NIL, where the PS was heated above its glass transition temperature while in contact with the mold. (iii) PSNTs were obtained upon mold removal. (c) SEM images of PSNTs with magnification of (i) 5000X, (ii) 25000X, and (iii) 80000X. (d) FIB-SEM image of a PSNT revealing the hollow cavity within.

To investigate the role of actin cytoskeleton and how that affects the delivery efficacy of PSNT-mediated delivery, we set up a time window before and after the cell–PSNT interface was established. For the *pre-interface* window, GPE86 cells were treated with Cyto D or Jas 12 h before the cell–PSNT interface was established; the drug treatment continued over the entire 6 h interfacing period. For the *post-interface* window, cells were seeded on mRNA-loaded PSNTs and cultured for 2 h, followed by incorporating the drugs into culture media for the rest 4 h of the interfacing period. GPE86 cells interfaced with mRNA-loaded PSNTs for the entire 6 h without drug addition were used as the untreated control. The cells were then characterized by means of SEM, confocal microscopy, and flow cytometry.

As cell viability is crucial for establishing a functional and biocompatible cell–NT interface, we examined the viability of GPE86 cells on PSNT using a live/dead viability assay. Flat PS substrates were used as a control. Confocal microscopy revealed the live (green) and dead (blue without green signal) cells on a representative PS substrate (Figure S2a). GPE86 cells on PSNTs displayed a high viability of 98%, similar to that on flat control of 97% (Figure S2b).

Next, we interfaced GPE86 cells on PSNT arrays under different treatment conditions, and characterized them by means of SEM. Distinctive morphological changes were observed in all the samples induced by both Cyto D and Jas for both treatment windows, as compared to the untreated cells (Figure 2a-c). The majority of the untreated cells were spreading substantially on the PSNTs, extending their filopodia and lamellipodia to establish NT contact, and even deforming the PSNTs (Figure 2a i-ii). In contrast, cells treated by either actin inhibitors exhibited significant changes in cell morphology (Figure 2b-c). Cyto D treated cells were rounded with very limited spreading on PSNTs for post- and pre-interface treatment (Figure 2b i-ii, 2b iii-iv, respectively). Formation of numerous membrane protrusions were observed on the surface of Cyto D treated cells—as sign of inhibition of the regular function of actin subunits.[71] Similarly, cells treated by Jas were also greatly hampered in their ability to spread on PSNTs, for both post- and pre-interface treatment (Figure 2c i-ii, 2c iii-iv, respectively). Cells in post-interface treatment also appeared to be affected by the drugs with some long protrusions forming on the spherical cell surface (Figure 2c ii). Both Cyto D and Jas treated samples also showed similar PSNT buckling like those on the untreated samples, due to the force exerted by the cell on the flexible PSNT.

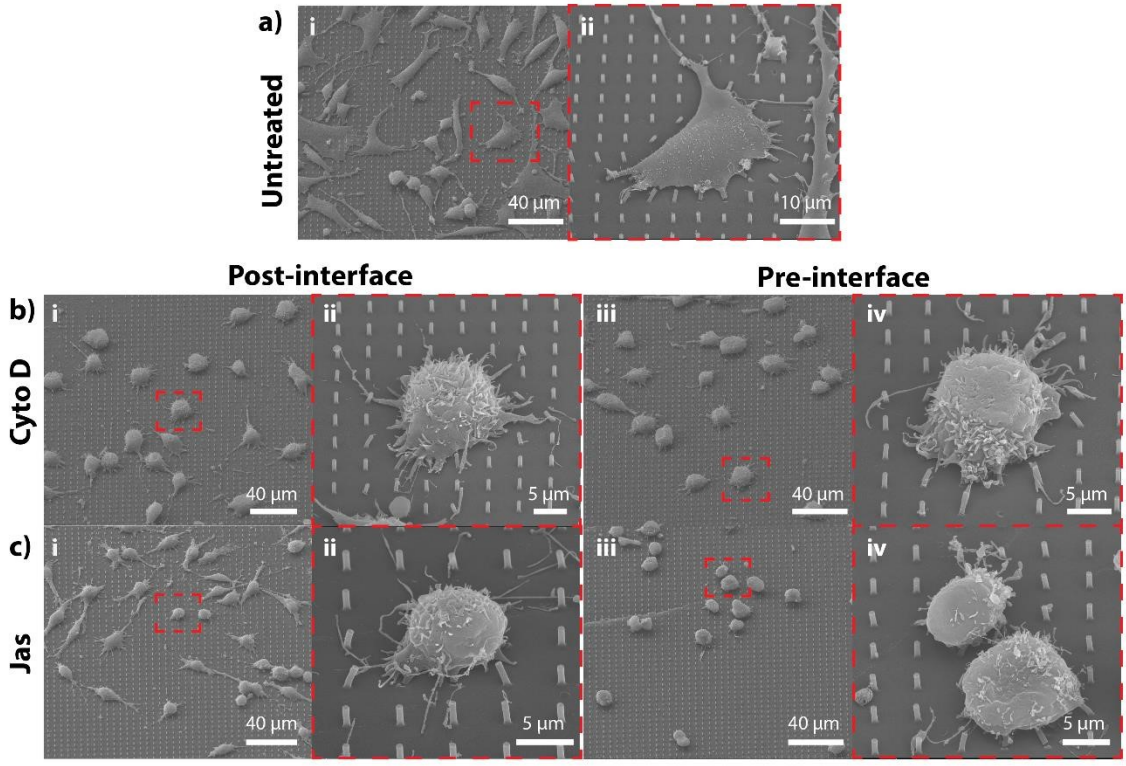

Figure 2. Effects of actin inhibitors on cell morphology on PSNTs. SEM images of (a) untreated GPE86 cells on PSNTs with (i) low and (ii) high magnification, (b) Cyto D- and (c) Jas-treated cells within the (i-ii) post-interface and (iii-iv) pre-interface treatment windows.

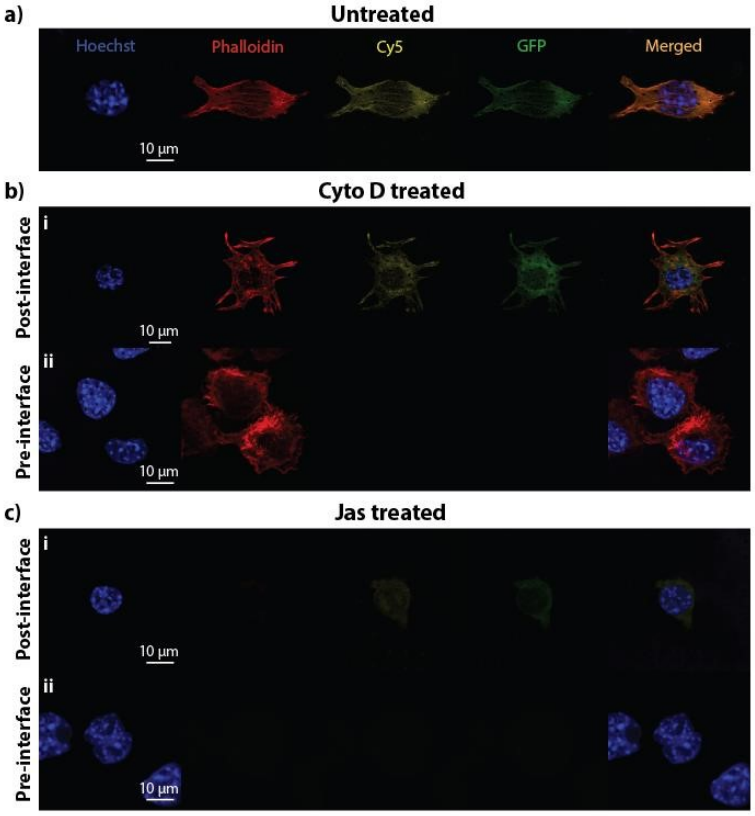

Figure 3. Effect of actin inhibitors on PSNT-mediated intracellular delivery. Confocal images of (a) untreated GPE86 cells and cells with pre- or post-interface treatment of (b) Cyto D or (c) Jas on PSNTs loaded with Cy5 (yellow)-tagged and GFP (green)-encoded mRNA after 6 h interfacing. Cells were stained with Hoechst (blue) and Phalloidin (red) to indicate nucleus and F-actin, respectively.

Using immunofluorescence detection via confocal microscopy and flow cytometry, we examined if the disruption of actin dynamics can influence PSNT-mediated mRNA delivery. The mRNA used in the experiment was Cy5-tagged and encoded with GFP; the insertion of mRNA into the cells can be indicated by Cy5 signal, and the successfully transfected cells will show GFP expression. Untreated GPE86 cells interfaced with mRNA-loaded PSNTs displayed Cy5 and GFP signals which indicated the successful mRNA delivery and transfection, with undisrupted F-actin meshwork observed by phalloidin staining (Figure 3a). Figure S3 shows an enlarged image of the F-actin meshwork of untreated and Cyto D-treated (post- and pre-interface) samples. The F-actin fibers on the untreated cell can be seen stretching across the cell and forming rings around the PSNTs (Figure S3a). In contrast, disruption of F-actin meshwork was observed in the post-interface Cyto D-treated cells (Figure S3b) and clustering of F-actin can be found within the pre-interface Cyto D-treated cells (Figure S3c). Surprisingly, cells both with post-interface Cyto D and Jas treatment gave similar results, despite their drastic alternation in morphology and F-actin network (Figure 3b i, 3c i). In contrast, GFP signals were barely noticeable in cells treated pre-interface by either of the two drugs (Figure 3b ii, 3c ii). We also observed extremely weak phalloidin staining in Jas-treated samples for both pre- and post-interface time windows (Figure 3c); this was expected as competitive binding between Jas and F-actin weakens the phalloidin staining capacity.[70] FIB-SEM imaging was used to further characterize the cross-sectional interface of cell–PSNT interaction. Untreated GPE86 cells formed a tight interface with PSNTs (Figure S4a), as well as both of the Cyto D- (Figure S4b) and Jas- (Figure S4c) treated samples regardless the treatment time windows. Both cell and nucleus membrane deformed around the PSNTs, with the resulting NTs being in close proximity to the nucleus. Interestingly, the untreated PSNTs were slightly compressed vertically after cell interfacing, in comparison to the actin inhibitor treated samples. Furthermore, the observation of broken SiNTs in our previous study treated by actin inhibitors were absent here,[14] where most of the PSNTs remained intact after cell interfacing. This is possibly due to the flexible nature of PSNTs to withstand force exerted by the cytoskeleton network that caused the buckling of SiNTs.

Quantification of the mRNA delivery efficiency was performed by detaching the cells from PSNTs after interfacing and analyzed using flow cytometry (Figure 4a). The delivery efficiency was measured by the populations of Cy5 positive cells, with average delivery efficiencies of ~83%, ~46%, and ~68% for untreated cells, post-interface Cyto D- and Jas-treated cells, respectively (Figure 4b). Notably, significant delivery efficiency reduction was observed in both pre-interface treatment, with delivery efficiency of only ~3% for Cyto D-treated samples and ~1% for Jas-treated samples. The normalized GFP geometric mean fluorescence intensity (GMFI) within the Cy5 positive cells revealed an enhancement of GFP

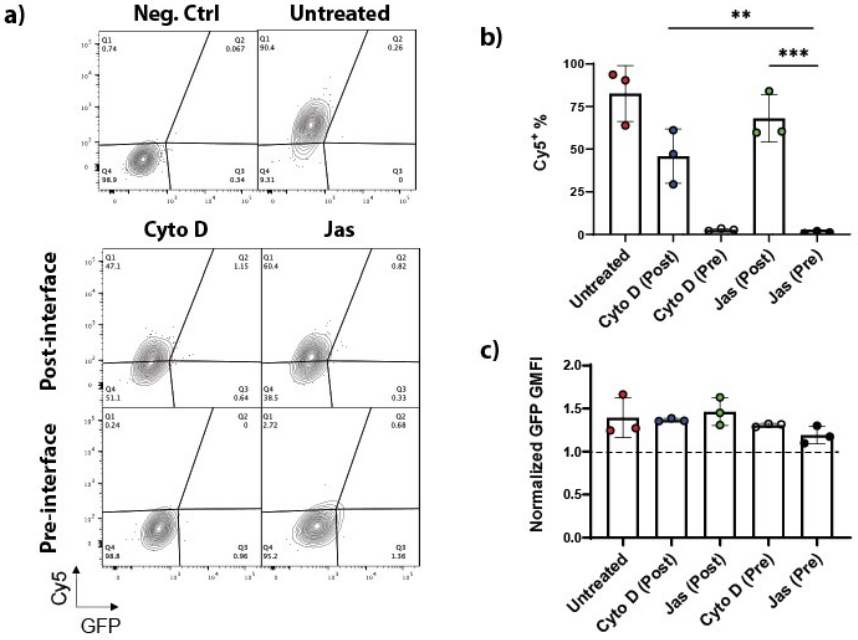

Figure 4. Quantitative analysis of PSNT-mediated mRNA delivery efficiency under different actin inhibitor treatment conditions. (a) Flow cytometry analysis showing Cy5 and GFP signals from untreated and pre-/post-interface Cyto D/Jas-treated GPE86 cells after detachment from PSNTs. (b) Quantification of $Cy5^+$ populations within detached GPE86 cells as in (a). (c) Quantification of normalized GFP GMFI within detached GPE86 cells as in (a) **$p \leq 0.0085$, ***$p \leq 0.0001$ (One-way ANOVA). n=3

signal (Figure 4c) compared to their respective controls, indicating the successful intracellular delivery has led to translation of mRNA into proteins. SiNT arrays have shown mRNA delivery efficiency of ~87% for untreated cells, ~85% for post-interface Cyto D-treated cells, and ~81% for post-interface Jas-treated cells.[14] By contrast, PSNT-mediated delivery has shown delivery efficiencies of ~83%, ~46%, and ~68% for untreated cells, post-interface Cyto D- and Jas-treated cells, respectively. Both SiNTs and PSNTs showed similar delivery efficiency for untreated cells based on Cy5 detection, but PSNTs showed limited GFP expression, possibly due to modulation of two independent input parameters: NT geometry and stiffness. Both have been proved to play a critical role in nanoinjection efficiency.[8, 38] Our previous study suggested that polymer nanoneedle-based nanoinjection is stiffness independent,[38] hence it is more likely that the geometrical differences between PSNTs and SiNTs have resulted in the discrepancy in GFP expression. Nanoinjection typically occurs within 1–2 h after the establishment of a stable cell–NN interface—possibly via the combination of penetration,[60, 61] enhanced endocytosis,[7, 37] and other biomechanical cues.[18, 62] But beyond this initial interfacing, endocytosis can still contribute to delivery to a lesser extent. This is aligned with our finding that (i) pre-interface treatment significantly lowered the delivery efficiency compared with post-interface-treated samples, but (ii) the delivery efficiency of post-interface-treated samples were still slightly reduced compared with that of the untreated control. This indicates that actin plays an important role in facilitating endocytosis. In summary, those results reflect the potential for using PSNT arrays as an effective nanoinjection platform in delivering mRNA into mammalian cells. It also reveals the importance of the actin cytoskeleton in polymer nanoneedle-based nanoinjection, suggesting that the majority of the PSNT-mediated delivery occurs at initial interfacing (≤2 h after establishing the interface). Induced pre-interface actin dysfunction reduces PSNT-mediated mRNA delivery efficiency much more than inhibiting actin post-interface.

Conclusions

We fabricated a novel PSNT array for mediating intracellular delivery of mRNA into GPE86 cells, and successfully achieved delivery efficiency of ~83% with untreated PSNTs. Actin dysfunction was induced by presenting Cyto D or Jas into the cell cultures at different time windows—pre-interface and post-interface. PSNT-mediated intracellular delivery of mRNA was significantly hindered when the actin cytoskeleton was disrupted prior PSNT-interfacing (~3% for Cyto D treated samples and ~1% for Jas treated samples). However, once the cell–PSNT interface had been established, the impact of actin inhibition on mRNA transfection efficiency was greatly reduced. This study also indicates that the initial 2 h interfacing period is crucial for successful delivery of bioactive cargos mediated by PSNT. In comparison to the stiff SiNTs, the flexible PSNTs were able to avoid breakage due to cellular forces at the interface. Overall, this sheds light on possible mechanism of polymeric NT-mediated delivery that involves functional actin, and demonstrates the potential of using polymeric materials—that is high-throughput, easy-to-fabricate pathway and relatively low cost—as a new class of nanoinjection platform.

Author Contributions

YC, NHV, and RE developed the idea for the study and its scope and supervised the experimental work. HZY and YC performed experiments and statistical data analyzing. A-RS assisted with SiNT master fabrication. HZY prepared the manuscript. HZY, YC, HT, NHV, and RE revised the manuscript. All the authors read and approved the final manuscript.

Conflicts of interest

There are no conflicts to declare

Funding

This work was supported by ARC DECRA (DE17010021) and ARC Future Fellowship (FT220100749), the ARC Training Centre for Personalized Therapeutics Technologies (IC170100016), Motherson Innovation, and CSIRO Manufacturing. Y.C., R.E. and N.H.V. acknowledge funding from Monash Institute of Pharmaceutical Sciences Commercialization Incubator Award, and the ARC Training Centre for Cell & Tissue Engineering Technologies (IC190100026) The research was conducted in part at the Melbourne Centre for Nanofabrication (MCN) in the Victorian Node of the Australian National Fabrication Facility (ANFF).

References

1. S. G. Higgins, M. Becce, A. Belessiotis-Richards, H. Seong, J. E. Sero and M. M. Stevens, *Advanced Materials*, 2020, **32**, 1903862.
2. Y. Chen, M. Alba, T. Tieu, Z. Tong, R. S. Minhas, D. Rudd, N. H. Voelcker, A. Cifuentes-Rius and R. Elnathan, *Advanced NanoBiomed Research*, 2021, **1**, 2100002.
3. A. F. McGuire, F. Santoro and B. Cui, *Annual Review of Analytical Chemistry*, 2018, **11**, 101-126.
4. H. Yoh, S. Aslanoglou, E. Lestrell, A.-R. Shokouhi, S. Belcher, H. Thissen, N. H. Voelcker and R. Elnathan, in *Semiconducting Silicon Nanowires for Biomedical Applications (Second Edition)*, ed. J. Coffer, Woodhead Publishing, 2022, DOI: https://doi.org/10.1016/B978-0-12-821351-3.00013-6, pp. 231-278.
5. R. Elnathan, A. Tay, N. H. Voelcker and C. Chiappini, *Nature Nanotechnology*, 2022, **17**, 807-811.
6. R. Elnathan, M. G. Barbato, X. Guo, A. Mariano, Z. Wang, F. Santoro, P. Shi, N. H. Voelcker, X. Xie, J. L. Young, Y. Zhao, W. Zhao and C. Chiappini, *Nature Reviews Materials*, 2022, **7**, 953-973.
7. S. Gopal, C. Chiappini, J. Penders, V. Leonardo, H. Seong, S. Rothery, Y. Korchev, A. Shevchuk and M. M. Stevens, *Advanced Materials*, 2019, **31**, 1806788.
8. R. Elnathan, B. Delalat, D. Brodoceanu, H. Alhmoud, F. J. Harding, K. Buehler, A. Nelson, L. Isa, T. Kraus and N. H. Voelcker, *Advanced Functional Materials*, 2015, **25**, 7215-7225.
9. I. Calaresu, J. Hernandez, R. Rauti, B. L. Rodilla, A. Arché-Núñez, L. Perez, J. Camarero, R. Miranda, M. T. González, I. Rodríguez, D. Scaini and L. Ballerini, *Advanced Materials Interfaces*, 2021, **8**, 2002121.
10. R. Elnathan, A. W. Holle, J. Young, M. A. George, O. Heifler, A. Goychuk, E. Frey, R. Kemkemer, J. P. Spatz, A. Kosloff, F. Patolsky and N. H. Voelcker, *Journal of Nanobiotechnology*, 2021, **19**, 51.
11. J. J. VanDersarl, A. M. Xu and N. A. Melosh, *Nano Letters*, 2012, **12**, 3881-3886.
12. L. Schmiderer, A. Subramaniam, K. Žemaitis, A. Bäckström, D. Yudovich, S. Soboleva, R. Galeev, C. N. Prinz, J. Larsson and M. Hjort, *Proc Natl Acad Sci U S A*, 2020, **117**, 21267-21273.
13. Y. Chen, S. Aslanoglou, T. Murayama, G. Gervinskas, L. I. Fitzgerald, S. Sriram, J. Tian, A. P. R. Johnston, Y. Morikawa, K. Suu, R. Elnathan and N. H. Voelcker, *Advanced Materials*, 2020, **32**, 2000036.
14. Y. Chen, H. Z. Yoh, A.-R. Shokouhi, T. Murayama, K. Suu, Y. Morikawa, N. H. Voelcker and R. Elnathan, *Journal of Nanobiotechnology*, 2022, **20**, 406.
15. S. Aslanoglou, Y. Chen, V. Oorschot, Z. Trifunovic, E. Hanssen, K. Suu, N. H. Voelcker and R. Elnathan, *Journal of the American Chemical Society*, 2020, **142**, 15649-15653.
16. Y. Chen, M. Mach, A.-R. Shokouhi, H. Z. Yoh, D. C. Bishop, T. Murayama, K. Suu, Y. Morikawa, S. C. Barry, K. Micklethwaite, R. Elnathan and N. H. Voelcker, *Materials Today*, 2023, DOI: https://doi.org/10.1016/j.mattod.2023.02.009.
17. A.-R. Shokouhi, S. Aslanoglou, D. Nisbet, N. H. Voelcker and R. Elnathan, *Materials Horizons*, 2020, **7**, 2810-2831.
18. R. Wen, A.-h. Zhang, D. Liu, J. Feng, J. Yang, D. Xia, J. Wang, C. Li, T. Zhang, N. Hu, T. Hang, G. He and X. Xie, *ACS Applied Materials & Interfaces*, 2019, **11**, 43936-43948.
19. Z. Liu, J. Nie, B. Miao, J. Li, Y. Cui, S. Wang, X. Zhang, G. Zhao, Y. Deng, Y. Wu, Z. Li, L. Li and Z. L. Wang, *Advanced Materials*, 2019, **31**, 1807795.
20. C. S. Hansel, S. W. Crowder, S. Cooper, S. Gopal, M. João Pardelha da Cruz, L. de Oliveira Martins, D. Keller, S. Rothery, M. Becce, A. E. G. Cass, C. Bakal, C. Chiappini and M. M. Stevens, *ACS Nano*, 2019, **13**, 2913-2926.
21. H.-Y. Lou, W. Zhao, Y. Zeng and B. Cui, *Accounts of Chemical Research*, 2018, **51**, 1046-1053.
22. H.-Y. Lou, W. Zhao, X. Li, L. Duan, A. Powers, M. Akamatsu, F. Santoro, A. F. McGuire, Y. Cui, D. G. Drubin and B. Cui, *Proceedings of the National Academy of Sciences*, 2019, **116**, 23143-23151.
23. J.-Y. Shiu, L. Aires, Z. Lin and V. Vogel, *Nature Cell Biology*, 2018, **20**, 262-271.
24. F. Tamzalit, M. S. Wang, W. Jin, M. Tello-Lafoz, V. Boyko, J. M. Heddleston, C. T. Black, L. C. Kam and M. Huse, *Science Immunology*, 2019, **4**, eaav5445.
25. F. Milos, A. Belu, D. Mayer, V. Maybeck and A. Offenhäusser, *Advanced Biology*, 2021, **5**, 2000248.
26. C. Chiappini, *ACS Sensors*, 2017, **2**, 1086-1102.
27. R. Kawamura, M. Miyazaki, K. Shimizu, Y. Matsumoto, Y. R. Silberberg, R. R. Sathuluri, M. Iijima, S. i. Kuroda, F. Iwata, T. Kobayashi and C. Nakamura, *Nano Letters*, 2017, **17**, 7117-7124.
28. Y. Chen, J. Wang, X. Li, N. Hu, N. H. Voelcker, X. Xie and R. Elnathan, *Advanced Materials*, 2020, **32**, 2001668.

29. C. Chiappini, E. De Rosa, J. O. Martinez, X. Liu, J. Steele, M. M. Stevens and E. Tasciotti, *Nature Materials*, 2015, **14**, 532-539.
30. Y. Cao, H. Chen, R. Qiu, M. Hanna, E. Ma, M. Hjort, A. Zhang, R. S. Lewis, J. C. Wu and N. A. Melosh, *Science Advances*, 2018, **4**, eaat8131.
31. H. Persson, J. P. Beech, L. Samuelson, S. Oredsson, C. N. Prinz and J. O. Tegenfeldt, *Nano Research*, 2012, **5**, 190-198.
32. P. Yang, S.-J. Chou, J. Li, W. Hui, W. Liu, N. Sun, R. Y. Zhang, Y. Zhu, M.-L. Tsai, H. I. Lai, M. Smalley, X. Zhang, J. Chen, Z. Romero, D. Liu, Z. Ke, C. Zou, C.-F. Lee, S. J. Jonas, Q. Ban, P. S. Weiss, D. B. Kohn, K. Chen, S.-H. Chiou and H.-R. Tseng, *Science Advances*, 2020, **6**, eabb7107.
33. H. Seong, S. G. Higgins, J. Penders, J. P. K. Armstrong, S. W. Crowder, A. C. Moore, J. E. Sero, M. Becce and M. M. Stevens, *ACS Nano*, 2020, **14**, 5371-5381.
34. A. M. Xu, S. A. Kim, D. S. Wang, A. Aalipour and N. A. Melosh, *Lab on a Chip*, 2016, **16**, 2434-2439.
35. A. K. Shalek, J. T. Gaublomme, L. Wang, N. Yosef, N. Chevrier, M. S. Andersen, J. T. Robinson, N. Pochet, D. Neuberg, R. S. Gertner, I. Amit, J. R. Brown, N. Hacohen, A. Regev, C. J. Wu and H. Park, *Nano Letters*, 2012, **12**, 6498-6504.
36. F. J. Harding, S. Surdo, B. Delalat, C. Cozzi, R. Elnathan, S. Gronthos, N. H. Voelcker and G. Barillaro, *ACS Applied Materials & Interfaces*, 2016, **8**, 29197-29202.
37. Y. Chen, S. Aslanoglou, G. Gervinskas, H. Abdelmaksoud, N. H. Voelcker and R. Elnathan, *Small*, 2019, **15**, 1904819.
38. H. Z. Yoh, Y. Chen, S. Aslanoglou, S. Wong, Z. Trifunovic, S. Crawford, E. Lestrell, C. Priest, M. Alba, H. Thissen, N. H. Voelcker and R. Elnathan, *Advanced Functional Materials*, 2022, **32**, 2104828.
39. A. Tay and N. Melosh, *Accounts of Chemical Research*, 2019, **52**, 2462-2471.
40. Y. Wang, Z. Wang, K. Xie, X. Zhao, X. Jiang, B. Chen, Y. Han, Y. Lu, L. Huang, W. Zhang, Y. Yang and P. Shi, *Nano Letters*, 2020, **20**, 5473-5481.
41. E. Lestrell, C. M. O'Brien, R. Elnathan and N. H. Voelcker, *Advanced Therapeutics*, 2021, **4**, 2100061.
42. S. Soltani Dehnavi, Z. Eivazi Zadeh, A. R. Harvey, N. H. Voelcker, C. L. Parish, R. J. Williams, R. Elnathan and D. R. Nisbet, *Advanced Materials*, 2022, **34**, 2108757.
43. M. Ermis, E. Antmen and V. Hasirci, *Bioactive Materials*, 2018, **3**, 355-369.
44. B. M. Rey, R. Elnathan, R. Ditcovski, K. Geisel, M. Zanini, M.-A. Fernandez-Rodriguez, V. V. Naik, A. Frutiger, W. Richtering, T. Ellenbogen, N. H. Voelcker and L. Isa, *Nano Letters*, 2016, **16**, 157-163.
45. C. Chiappini, in *Handbook of Porous Silicon*, ed. L. Canham, Springer International Publishing, Cham, 2018, DOI: 10.1007/978-3-319-71381-6_17, pp. 247-267.
46. D. Brodoceanu, H. Z. Alhmoud, R. Elnathan, B. Delalat, N. H. Voelcker and T. Kraus, *Nanotechnology*, 2016, **27**, 075301.
47. L. Scheidegger, M. Á. Fernández-Rodríguez, K. Geisel, M. Zanini, R. Elnathan, W. Richtering and L. Isa, *Physical Chemistry Chemical Physics*, 2017, **19**, 8671-8680.
48. R. Elnathan, L. Isa, D. Brodoceanu, A. Nelson, F. J. Harding, B. Delalat, T. Kraus and N. H. Voelcker, *ACS Applied Materials & Interfaces*, 2015, **7**, 23717-23724.
49. H. Alhmoud, D. Brodoceanu, R. Elnathan, T. Kraus and N. H. Voelcker, *Progress in Materials Science*, 2021, **116**, 100636.
50. H. Kim, H. Jang, B. Kim, M. K. Kim, D. S. Wie, H. S. Lee, D. R. Kim and C. H. Lee, *Science Advances*, 2018, **4**, eaau6972.
51. C. Chiappini and C. Almeida, in *Semiconducting Silicon Nanowires for Biomedical Applications*, ed. J. L. Coffer, Woodhead Publishing, 2014, DOI: https://doi.org/10.1533/9780857097712.2.144, pp. 144-167.
52. J. Carthew, H. H. Abdelmaksoud, K. J. Cowley, M. Hodgson-Garms, R. Elnathan, J. P. Spatz, J. Brugger, H. Thissen, K. J. Simpson, N. H. Voelcker, J. E. Frith and V. J. Cadarso, *Advanced Functional Materials*, 2022, **32**, 2100881.
53. J. Carthew, H. H. Abdelmaksoud, M. Hodgson-Garms, S. Aslanoglou, S. Ghavamian, R. Elnathan, J. P. Spatz, J. Brugger, H. Thissen, N. H. Voelcker, V. J. Cadarso and J. E. Frith, *Advanced Science*, 2021, **8**, 2003186.
54. K. S. Beckwith, S. P. Cooil, J. W. Wells and P. Sikorski, *Nanoscale*, 2015, **7**, 8438-8450.
55. H. Hubbe, E. Mendes and P. E. Boukany, *Micromachines*, 2019, **10**, 225.
56. G. Tullii, F. Giona, F. Lodola, S. Bonfadini, C. Bossio, S. Varo, A. Desii, L. Criante, C. Sala, M. Pasini, C. Verpelli, F. Galeotti and M. R. Antognazza, *ACS Applied Materials & Interfaces*, 2019, **11**, 28125-28137.
57. C. Chiappini, Y. Chen, S. Aslanoglou, A. Mariano, V. Mollo, H. Mu, E. De Rosa, G. He, E. Tasciotti, X. Xie, F. Santoro, W. Zhao, N. H. Voelcker and R. Elnathan, *Nature Protocols*, 2021, **16**, 4539-4563.
58. G. He, N. Hu, A. M. Xu, X. Li, Y. Zhao and X. Xie, *Advanced Functional Materials*, 2020, **30**, 1909890.
59. E. Lestrell, F. Patolsky, N. H. Voelcker and R. Elnathan, *Materials Today*, 2020, **33**, 87-104.
60. C. Chiappini, J. O. Martinez, E. De Rosa, C. S. Almeida, E. Tasciotti and M. M. Stevens, *ACS Nano*, 2015, **9**, 5500-5509.
61. D. Matsumoto, A. Yamagishi, M. Saito, R. R. Sathuluri, Y. R. Silberberg, F. Iwata, T. Kobayashi and C. Nakamura, *Journal of Bioscience and Bioengineering*, 2016, **122**, 748-752.
62. G. C. Messina, M. Dipalo, R. La Rocca, P. Zilio, V. Caprettini, R. Proietti Zaccaria, A. Toma, F. Tantussi, L. Berdondini and F. De Angelis, *Advanced Materials*, 2015, **27**, 7145-7149.
63. L. Lanzetti, *Current Opinion in Cell Biology*, 2007, **19**, 453-458.
64. A. Aalipour, A. M. Xu, S. Leal-Ortiz, C. C. Garner and N. A. Melosh, *Langmuir*, 2014, **30**, 12362-12367.
65. R. Kawamura, K. Shimizu, Y. Matsumoto, A. Yamagishi, Y. R. Silberberg, M. Iijima, S. Kuroda, K. Fukazawa, K. Ishihara and C. Nakamura, *Journal of Nanobiotechnology*, 2016, **14**, 74.
66. T. C. von Erlach, S. Bertazzo, M. A. Wozniak, C.-M. Horejs, S. A. Maynard, S. Attwood, B. K. Robinson, H. Autefage, C. Kallepitis, A. del Río Hernández, C. S. Chen, S. Goldoni and M. M. Stevens, *Nature Materials*, 2018, **17**, 237-242.
67. B. G. Nair, K. Hagiwara, M. Ueda, H.-h. Yu, H.-R. Tseng and Y. Ito, *ACS Applied Materials & Interfaces*, 2016, **8**, 18693-18700.

68. W. Zhao, L. Hanson, H.-Y. Lou, M. Akamatsu, P. D. Chowdary, F. Santoro, J. R. Marks, A. Grassart, D. G. Drubin, Y. Cui and B. Cui, *Nature Nanotechnology*, 2017, **12**, 750-756.
69. M. Trendowski, *Anticancer Agents Med Chem*, 2015, **15**, 327-335.
70. A. Holzinger, in *Cytoskeleton Methods and Protocols*, ed. R. H. Gavin, Humana Press, Totowa, NJ, 2010, DOI: 10.1007/978-1-60761-376-3_4, pp. 71-87.
71. D. S. Gokhin, R. B. Nowak, J. A. Khoory, A. d. l. Piedra, I. C. Ghiran and V. M. Fowler, *Molecular Biology of the Cell*, 2015, **26**, 1699-1710.